FALL 2023
electronics-cooling.com

electronics COOLING

FEATURED IN THIS EDITION

13 REVOLUTIONIZING DATA CENTER SUSTAINABILITY WITH INTELLIGENT, PURPOSE-BUILT SOLUTIONS

16 EXPERIMENTAL EVALUATION OF SUPERCRITICAL CARBON DIOXIDE AS A VIABLE COOLANT FOR ELECTRONICS THERMAL MANAGEMENT

20 MACHINES NOW FILL AND PERCEIVE SCENES FOR SCIENTISTS AND ENGINEERS

9 CALCULATION CORNER
CALCULATING THERMAL DESIGN POWER FOR MOBILE CONSUMER ELECTRONICS – PART 3

26 STATISTICS CORNER
BAD DATA!

LEADER TECH
a HEICO company

THE LEADING EDGE IN EMI/RFI SHIELDING TECHNOLOGY

YOUR SOURCE FOR THERMAL INTERFACE MATERIALS

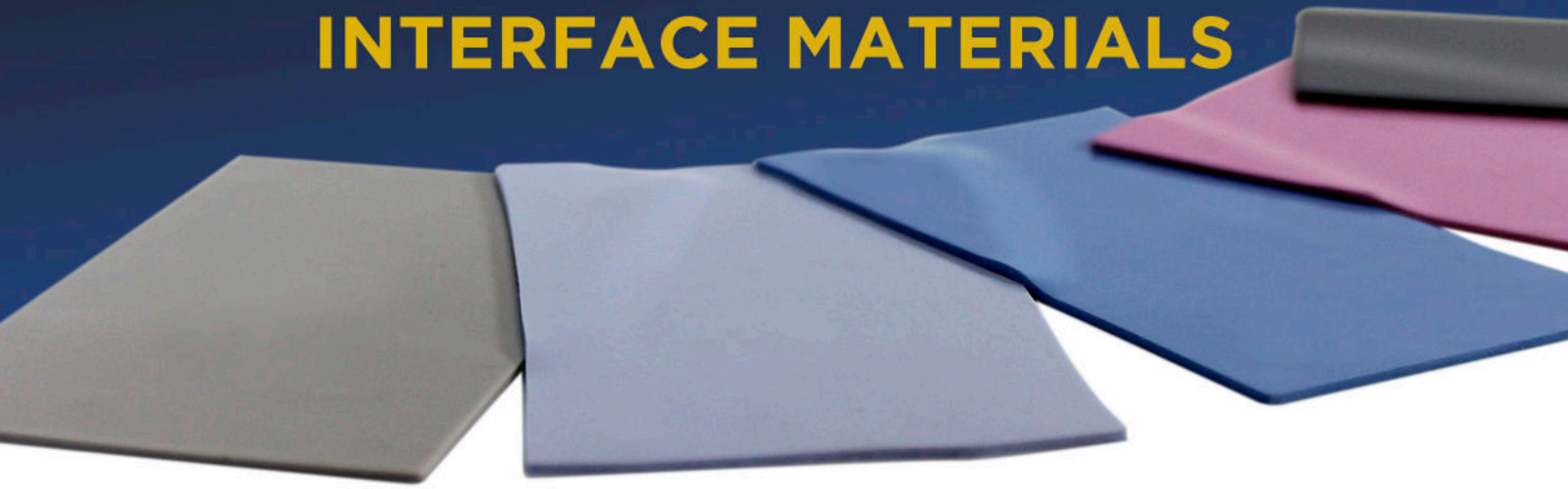

Leader Tech serves a diverse commercial and military customer base from its Global EMI Shielding Technology Center located in Tampa, Florida. Every detail of the company's one-of-a-kind manufacturing facility is tailor-engineered to streamline and improve customer service, engineering and manufacturing processes. We are committed to the US market by expanding our industry experienced team, innovative manufacturing technology and US based facility.

- **Thermally Conductive Graphite**
- **Thermal Grease/Gel Series**
- **Thermally Conductive Electrical Insulators**
- **Thermal Conductive Double-sided Adhesive**

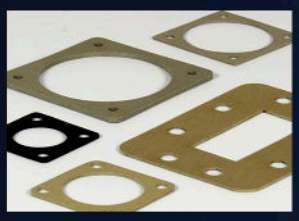
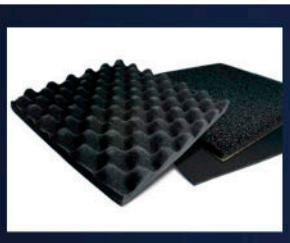


Visit us, follow us, watch us, and connect with us at:

Email: sales@leadertechinc.com
12420 Race Track Rd Tampa, Florida 33626
www.leadertechinc.com

ISO 9001 QUALITY MANAGEMENT

ANAB ACCREDITED MANAGEMENT SYSTEMS CERTIFICATION BODY

ITAR

CONTENTS

electronics COOLING
electronics-cooling.com

4 **EDITORIAL**
Genevieve Martin

6 **TECHNICAL EDITORS SPOTLIGHT**

7 **COOLING EVENTS**
News of Upcoming 2023/2024 Thermal Management Events

9 **CALCULATION CORNER**
Calculating Thermal Design Power for Mobile Consumer Electronics – Part 3
Alex Ockfen

13 **REVOLUTIONIZING DATA CENTER SUSTAINABILITY WITH INTELLIGENT, PURPOSE-BUILT SOLUTIONS**
Mukul Anand

16 **EXPERIMENTAL EVALUATION OF SUPERCRITICAL CARBON DIOXIDE AS A VIABLE COOLANT FOR ELECTRONICS THERMAL MANAGEMENT**
Wyatt Stottlemyre, Alec Nordlund, Joshua Gess
Bharath Ramakrishnan, Husam Alissa

20 **MACHINES NOW FILL AND PERCEIVE SCENES FOR SCIENTISTS AND ENGINEERS**
Nhi Quach, Youngjoon Suh, Jewoo Park, Yoonjin Won

26 **STATISTICS CORNER**
Bad Data!
Ross Wilcoxon

30 **INDEX OF ADVERTISERS**

PUBLISHED BY
Lectrix
716 Dekalb Pike, #351
Blue Bell, PA 19422
Phone: +1 484-688-0300; Fax:+1 484-688-0303
info@lectrixgroup.com
lectrixgroup.com

CHIEF EXECUTIVE OFFICER
Graham Kilshaw | graham@lectrixgroup.com

DIRECTOR OF MEDIA & EVENTS
Katherine Struve | katherine@lectrixgroup.com

DIRECTOR OF BUSINESS DEVELOPMENT
Ashlee Zapata-McCants | ashlee@lectrixgroup.com

CREATIVE DIRECTOR
Kate Teti | kate@lectrixgroup.com

GRAPHIC DESIGNER
Marcos Cruz | marcos@lectrixgroup.com

DIRECTOR OF OPERATIONS & CULTURE
Stephanie Curry | stephanie@lectrixgroup.com

DELIVERY MANAGER
Mackenzie Mann | mackenzie@lectrixgroup.com

►SUBSCRIPTIONS ONLINE
at electronics-cooling.com

For subscription changes email
info@electronics-cooling.com

FREE SUBSCRIPTIONS

Lectrix®, Electronics Cooling®—The **2023 Fall Edition** is distributed digitally at no charge to engineers and managers engaged in the application, selection, design, test, specification or procurement of electronic components, systems, materials, equipment, facilities or related fabrication services. Subscriptions are available through electronics-cooling.com.

LECTRIX

EDITORIAL

Genevieve Martin
Associate Technical Editor of *Electronics Cooling Magazine*
R&D Manager for Thermal & Mechanics

Embracing the Future: How AI and Generative Gesign Reshape High Tech Competence.

In the wake of unprecedented challenges like Covid pandemic, the ongoing Ukraine war, and the resulting component shortage, industries worldwide are showing remarkable resilience. As we stand at the precipice of a new era, all sectors are poised to take a giant leap forward.

The buzzword on everyone's lips is no longer Industry 4.0; instead it's Artificial Intelligence (AI), which is expected to revolutionize the industry landscape. With the advent of AI and generative design, the industry is on an exploratory journey that promises to redefine our competence, capabilities, way of working and software tooling.

I recently found myself deeply involved in updating our company's thermal management and mechanics technology funnel, aiming to identify most pertinent new technologies to our business. Along with the identification of potentially relevant technologies, I analyse the disruptive trends touching almost all industries. To name a few:

- Electronics – Industry remains dominated with the continuous increase of electronics/sensors. Electronics are still on today's agenda.
- Growth of additive manufacturing – 3D printing is re-shaping the manufacturing industry.
- Digital transformation is still progressing – Software suppliers start to focus on fully embedded tool suite, running simulation with embedded Digital twins, adoption of AI in the tool suite
- Sustainability – Suppliers start to consider sustainability in their solutions e.g. easy recyclability, saving of resources, refurbishment, re-use
- Towards resilient systems – Uncertainties at the supply chain leads to incorporate the potential for disruption, make system simpler

As the era for digitalisation and sustainability unfolds, we seek enhanced performance while striving to remain at the vanguard of innovation. Excitingly, Digital twins and new manufacturing processes such as 3D-printing have opened doors to a plethora of possibilities, ushering in a new era of product development.

One article that aroused my attention was "Shift left, Extend right, Stretch sideways", by Brian Bailey, published in SemiconductorEngineering. It resonated with my thoughts on the ongoing technological upheaval and its potential impact on our collaboration, way of working. Moreover, "Don't panic – the potential impact of Large Language Models (LLMs) on Computer Aided Engineering", an insightful Linkedin post by Robin Bornoff, beautifully encapsulated our current position and the challenges that lie ahead.

But amidst this transformational landscape, the burning question remains: How will AI, ChatGPT, and Generative design impact our product development process? What might be their implications on electronics development and on thermal management?

AI and generative design have the potential to revolutionize the way we conceive, design, and manufacture products. They empower us to unlock unprecedented levels of efficiency, creativity, and innovation. By leveraging AI and generative design, engineers can explore countless design possibilities at an incredible pace. This accelerated ideation process can lead to new breakthroughs that the human mind alone might not have envisioned.

The implications extend far beyond efficiency gains. Our cooling of the electronics field, crucial in today's and future products, stands to benefit significantly from these technological advancements. As a result, we can push the boundaries of performance and design complexity handling without compromising on sustainability or innovation.

However, as with any technological leap, there are challenges and ethical considerations to address. While AI can generate designs quickly, humans still bring creativity, judgement to the design process. Besides, as AI generates numerous design options, ethical considerations might arise. For instance, a design might be unsafe for users, not adhere to environmental or social standards. As we embrace AI and generative design, we must ensure that we maintain a balance between human creativity and automation.

As the high-tech industry moves forward, embracing these transformative technologies with a mindful approach will undoubtedly shape the future of our competence: collaboration, knowledge sharing, and continuous learning will be key to harnessing the full potential of AI and generative design.

As always, we editors welcome your feedback and invite you to submit your own article to be included in a future issue.

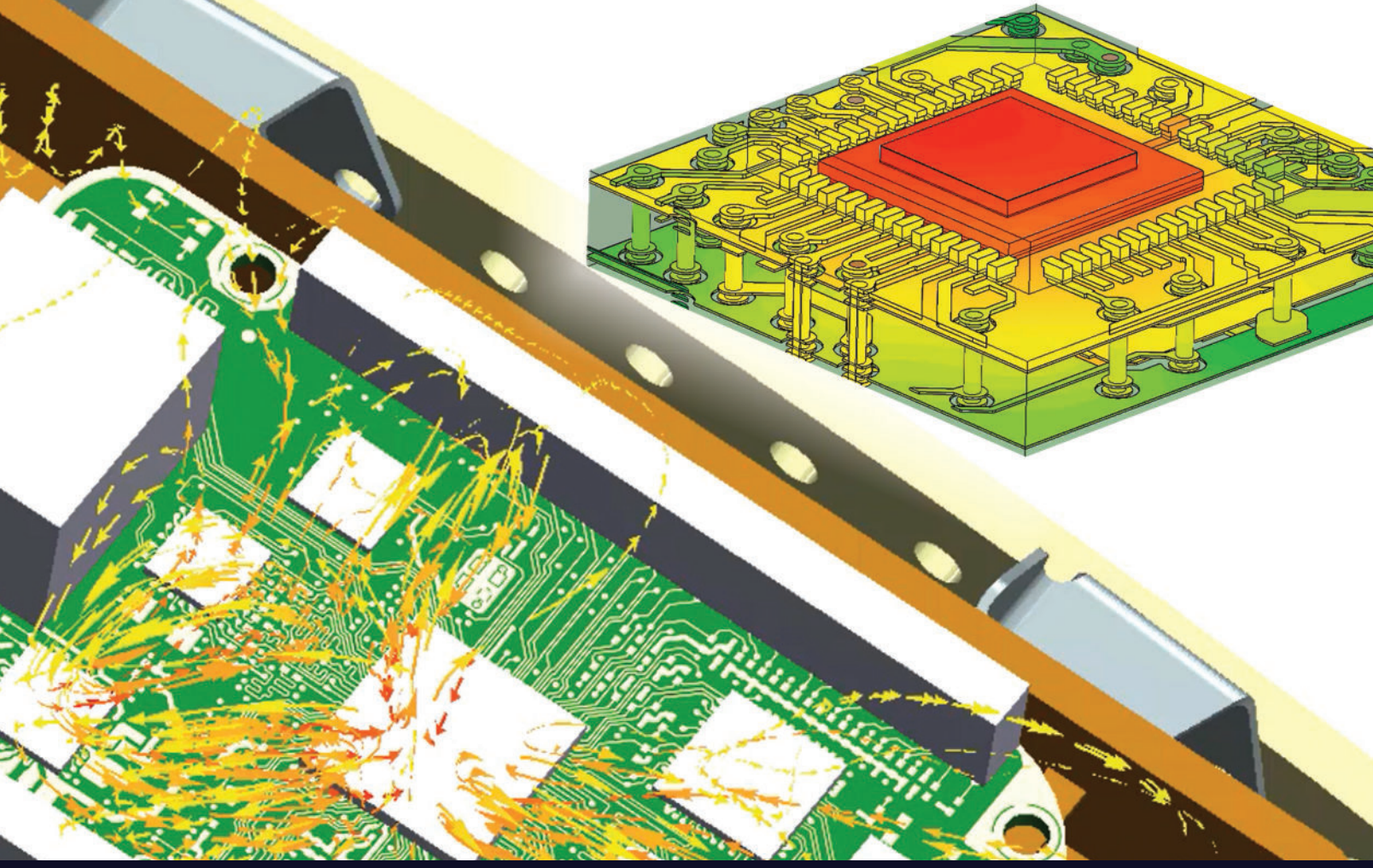

Accelerate thermal, thermo-mechanical and electro-thermal workflows

Leverage efficient CFD and FEA workflows for shorter, robust thermal and thermo-mechanical analysis. Underpin simulation accuracy with thermal measurement for characterization, calibration to reliability assessment. Incorporate EDA and MCAD data complexity efficiently into simulation. Enable PCB electro-thermal modeling using power integrity co-simulation. Realize the advantage of novel reduced order thermal model generation from full 3D analysis to improve accuracy in circuit or system modeling.

Simcenter provides simulation and test solutions to support you in developing a thermal digital twin. The portfolio includes a range of leading electronics cooling software , CAD-embedded CFD simulation options, and multi-physics analysis tools to support a wider range of user skill and experience demographic from analyst to designer. Learn how Siemens Digital Industries Software can help you achieve digital transformation goals.

www.siemens.com/simcenter

SIEMENS

TECHNICAL EDITORS SPOTLIGHT

Meet the 2023 Editorial Board

VICTOR CHIRIAC, PhD | GLOBAL COOLING TECHNOLOGY GROUP

Associate Technical Editor

A fellow of the American Society of Mechanical Engineers (ASME) since 2014, Dr. Victor Adrian Chiriac is a co-founder and a managing partner with the Global Cooling Technology Group since 2019. He previously held technology/engineering leadership roles with Motorola (1999-2010), Qualcomm (2010 – 2018) and Huawei R&D USA (2018 – 2019). Dr. Chiriac was elected Chair of the ASME K-16 Electronics Cooling Committee and was elected the Arizona and New Mexico IMAPS Chapter President. He is a leading member of the organizing committees of ASME/InterPack, ASME/ IMECE and IEEE/CPMT Itherm Conferences. He holds 21 U.S. issued patents, 2 US Trade Secrets and 1 Defensive Publication (with Motorola), and has published over 110 papers in scientific journals and at conferences.

► vchiriac@gctg-llc.com

GENEVIEVE MARTIN | SIGNIFY

Associate Technical Editor

Genevieve Martin (F) is the R&D manager for thermal & mechanics competence at Signify (former Philips Lighting), The Netherlands. She has worked in the field of cooling of electronics and thermal management for over twenty years in different application fields. From 2016 to 2019, she coordinated the European project Delphi4LED, which dealt with multi-domain compact modeling of LEDs and, since 2021, is coordinating the AI-TWILIGHT project. She served as general chair of the SEMI-THERM conference and is an active reviewer and technical committee member in key conferences including SEMI-THERM, Therminic, and Eurosime. She has over 20 journal and conference papers and 16 worldwide patents.

► genevieve.martin@signify.com

ALEX OCKFEN, P.E. | META

Associate Technical Editor

Alex Ockfen is a simulation engineer at Meta (formerly Facebook), providing technical leadership for thermal and structural design of consumer electronics products. He held previous positions at Raytheon where he obtained experience in thermal management and electronics cooling of a wide range of aerospace and defense applications. He has more than 10 journal and conference publications, is an inventor on multiple patents, is a professional mechanical engineer, and is currently serving as program chair of the SEMI-THERM conference.

► alex.ockfen@fb.com

ROSS WILCOXON | COLLINS AEROSPACE

Associate Technical Editor

Dr. Ross Wilcoxon is a Senior Technical Fellow in the Collins Aerospace Advanced Technology group. He conducts research and supports product development in the areas of component reliability, electronics packaging, and thermal management for communication, processing, displays, and radars. He has more than 40 journal and conference publications and is an inventor on more than 30 US Patents. Prior to joining Rockwell Collins (now Collins Aerospace) in 1998, he was an assistant professor at South Dakota State University.

► ross.wilcoxon@collins.com

COOLING EVENTS

News of Upcoming 2023/2024 Thermal Management Events

DEC
5-7

Thermal Management Expo Europe
Stuttgart, Germany

Part of the global Thermal Management Expo portfolio, Thermal Management Expo Europe is the only free to attend cross-sector exhibition and conference connecting senior engineers and decision makers with suppliers of thermal systems and materials. It's a unique opportunity for professionals in the Automotive, aerospace & Defence, electronics, energy, Telecoms/5G, and medical sectors to discuss the latest thermal innovations and solutions, benefiting from cross-sector networking and in-person interaction with the latest materials, components, and technologies available in the thermal marketplace.

Desc. source: electronics-cooling.com
►**thermalmanagementexpo-europe.com**

MAY
7

Thermal Live Spring Summit 2024
Virtual

Thermal Live Spring Summit 2024 is an online, one-day event that is your chance to hear from thermal management experts on current trends, product updates, and concepts explained. Join Electronics Cooling for a day to enhance your craft and be in the know!

Desc. source: electronics-cooling.com
►**thermal.live**

MAY
23

Battery Thermal Management Innovation
Paulo Alto, California

Battery Thermal Management Innovation USA is the #1 and most revered conference&exhibition to match OEM and Battery Manufacturer requirements with expert material, solution, and technology providers. Following the series' success over the previous four instalments in California the show has continued to grown and has become know as the industry's best-in-class and foremost communication network for BTM practitioners. BTM Innovation USA is North Americas leading event for battery thermal management engineers, technologists, and experts to collectively address the key challenges and industry innovations surrounding advanced battery thermal management systems, materials, technologies, and solutions; to increase efficiency, range battery health, and optimizes solutions for increasingly demanding, ever advancing battery requirements. The conference analyses innovative battery management solutions, explores the most crucial engineering and material challenges and benchmarks strategic imperatives for next-generation BEV advancement. We welcome you to join over 400 xEV experts at North Americas largest technical conference for battery thermal management professionals and foremost communication network for OEMs, technology and solutions providers alike; where experts will engage during a series of case study presentations, interactive panels and unparalleled networking opportunities.

Desc. source: electronics-cooling.com
►**battery-thermal-management-usa.com**

SEMI-THERM®

40th Annual Semiconductor Thermal Measurement, Modeling and Management Symposium

March 25-29, 2024 | San Jose, CA, US

Register now at semi-therm.org

Keynote Speaker

TIM SHEDD

Engineering Technologist, Office of the CTIO at Dell, **Tim Shedd** will share his insights on the topic "Driving Sustainable Scaling of Compute to 2030"

Expand your expertise with the top-rated short courses!

"Thermal Challenges and Opportunities of Advanced Packages and Microelectronics Systems. Figure of Merit and Applications." Dr. Victor Chiriac (Global Cooling Technolog Group), Alex Ockfen (Meta)

"Direct to Chip Liquid Cooling: Single Phase Water and Two-Phase Refigerant Cooling with Pumped and Passive Systems" Professor Alfonso Ortega (Villanova University), Dr. Luca Amalfi (Seguente Inc.)

"Fundamentals and Applications of Machine Learning in Thermal Management and Heat Transfer Technologies" Professor Van P. Carey (UC Berkeley), Professor Alanna Cooney (San Francisco State Univerity)

"Semiconductor Packaging and Thermals: Upcoming Challenges" Dr. Kyle Arrington (Intel)

"Navigating Thermal and Reliability Challenges in Chip Components for Automotive High-Performance Compute Systems" Dr. Fen Chen (Cruise, LLC)

"Transient Thermal Analysis Using Linear Superposition" Roger Stout (Professional Engineer, Retired)

"Passive Two-Phase Cooling: Pulsating Heat Pipes and Loop Thermosyphons" Professor Emeritus John Thome (JJ Cooling Innovation Sàrl)

SPONSORS

Platinum

celsia™ Making Hot Technology Cooler

Diabatix

Short course

ARIECA

Media

electronics COOLING

View the complete program at semi-therm.org

Calculating Thermal Design Power for Mobile Consumer Electronics – Part 3

Alex Ockfen, P.E.
Simulation Engineer at Meta

Overview

Thermal Design Power (TDP) is a term commonly used in thermal management of consumer electronics. While the usage of this terminology may vary across the industry, it commonly refers to the amount of power that a device may dissipate indefinitely, in a given thermal environment, without exceeding the temperature limits of the device. The TDP for a consumer electronics device is of great interest because it provides physical bounds to the experience a product can deliver to the user (e.g., phone call, internet, photo capture, gaming, etc.).

Thermal design engineers often have the most influence on a product's design during its architecture development. It is not uncommon for designs to rapidly evolve in this phase of the design cycle, with real-time changes occurring daily or even hourly. Some first-order tools are essential to provide effective thermal design guidance in a fast-paced environment. Detailed finite element or computational fluid dynamics simulations are often not practical due to the timeline and lack of design maturity. TDP provides one simple and useful metric that can guide the design in the desired direction.

Where We Left Off

Physics-based methods for determining the thermal design power of a passively cooled consumer electronics device have been developed. The thermal design power of a device like that shown in *Figure 1* is typically calculated using *equation 1*, where h is the effective heat transfer coefficient, A is the external area of the device, T_{limit} is the touch temperature limit, $T_{ambient}$ is the ambient operating temperature, and the CTS is the coefficient of thermal spreading [1].

$$TDP = hA(T_{limit} - T_{ambient})CTS \qquad \{1\}$$

The coefficient of thermal spreading is a term that accounts for any spatial temperature gradients over the surface of the device. This term is typically between 0.5 and 0.8 for consumer electronics devices, with a value of 1.0 representing the ideal isothermal device.

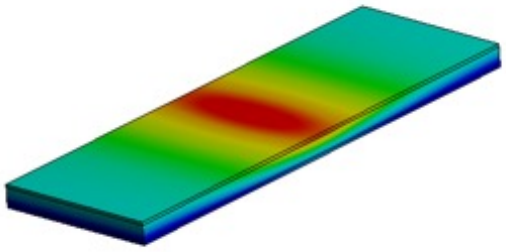

Figure 1 - Isotherm on an example tablet or mobile phone product

Part 1 of this column provided a method to calculate the CTS for thermal gradients in the plane of the device [3], while Part 2 provided a method to calculate the CTS for thermal gradients through the thickness of the device [4]. These methods will be briefly summarized in the following sections, then they will be combined to provide the thermal design engineer with a CTS calculation methodology that enables them to simultaneously capture the effects of both in-plane and through-plane temperature gradients on thermal design power.

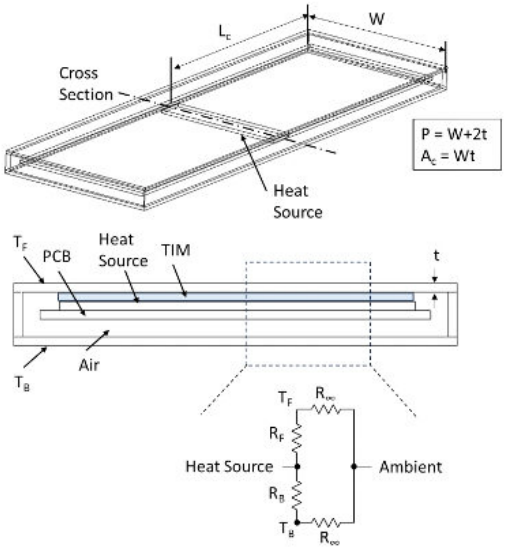

Figure 2 - Example geometry of a product for demonstrating TDP calculations

In-Plane Thermal Gradients

Figure 2 defines the general construction and geometry of the consumer electronics device used to illustrate the thermal design power calculation. While a notional design with the heat source along the centerline of the device is shown here, the approach is general, and the practicing engineer may adjust the parameters to fit their specific needs.

The large aspect ratio of mobile phones and tablets is reminiscent of a fin. Thus, an in-plane coefficient of thermal spreading can be calculated using *equation 2*, where η is the fin efficiency, L_c is the characteristic length, and m is defined via *equation 3*.

$$\eta = \frac{tanh\, mL_c}{mL_c} \quad \{2\}$$

The quantity m is a function of the fin perimeter (P), cross-sectional area (A_c), effective conductivity of the device housing (k_{eff}), and the heat transfer coefficient (h). The heat transfer coefficient in this equation can be chosen using empirical correlations and should account for both convection and radiation.

$$m = \sqrt{\frac{hP}{k_{eff}A_c}} \quad \{3\}$$

Through-Plane Thermal Gradients

A through-plane coefficient of thermal spreading can be calculated using a parallel resistance network as shown in *Figure 2*, where the thermal resistance values from the heat source to the front (R_F) and back (R_B) surfaces of the device define the heat transfer split and through-plane temperature differential. These resistance values can be calculated using the standard resistance formulas for conduction and convection as provided in *equation 4*.

$$R_{cond} = \frac{L}{kA_{conduction}}, R_{conv} = \frac{1}{hA_{convection}} \quad \{4\}$$

Solution of the parallel resistor network yields the thermal spreading multiplier ($M^*_{through\text{-}plane}$), defined in *equation 5*, where R_∞ is the thermal resistance between the device surface and the external environment. R_∞ is calculated based on the full surface area of one side of the device (front or back only). Note that this multiplier includes the in-plane fin efficiency which is required when in-plane temperature gradients are present and influence resistance to ambient. This fin efficiency parameter was not included in reference [4] because no in-plane temperature gradients were assumed in that effort.

$$M^*_{through-plane} = \frac{1}{1+\frac{ABS(R_B-R_F)}{(R_B+R_F+2R_\infty/\eta)}} \quad \{5\}$$

Two additional equations are provided to enable a non-dimensional formulation and enable generic design plots against the quantity R_{eq}/R_{max}. R_{eq} is defined by *equation 6* and represents the total equivalent thermal resistance from the heat source to the environment (including both front and back surfaces). R_{max} is defined by *equation 7* and represents the larger of the thermal resistances between the heat source and the environment (through either the front or back surfaces individually).

$$R_{eq} = \frac{(R_B+R_\infty)(R_F+R_\infty)}{(R_B+R_F+2R_\infty)} \quad \{6\}$$

$$R_{max} = MAX[(R_B + R_\infty), (R_F + R_\infty)] \quad \{7\}$$

Bringing It All Together

It is typically not practical to design a device with either perfect in-plane thermal spreading or with a perfect heat balance between the front and back surfaces. Thus, it is useful to extend the equation for the coefficient of thermal spreading to include both the in-plane and through-plane contributions previously discussed.

The combined coefficient of thermal spreading calculation is provided in *equation 8* and is obtained by multiplying the fin efficiency (η) from *equation 2* and the through-plane multiplier ($M^*_{through\text{-}plane}$) from *equation 5*.

$$CTS = \eta M^*_{through-plane} = \frac{\tanh(mL_c)/mL_c}{1+\frac{ABS(R_B-R_F)}{(R_B+R_F+2R_\infty/\eta)}} \quad \{8\}$$

Figure 3 illustrates the coefficient of thermal spreading as a function of the non-dimensional design parameters governing in-plane ($1/mL_c$) and through-plane (R_{eq}/R_{max}) thermal performance. The CTS is shown to be most sensitive to in-plane thermal spreading and can approach zero when $1/mL_c$ approaches zero. This can occur when either the effective thermal conductivity of the housing becomes small, or the device becomes large (compared to heat source size). The importance of through-plane heat spreading is also apparent as a near-ideal in-plane design ($1/mL_c$ = 5) may yield a coefficient of thermal spreading of 0.5 if there is an extreme imbalance in the thermal resistance between the heat source and the front and back surfaces of the device.

We can now reframe the data to make it more useful for the thermal design engineer. Thermal design power targets are commonly known and can be easily translated into a target CTS value using *equation 1*. *Figure 4* provides design curves for multiple target CTS values. Each curve provides a set of design combinations that can be selected to achieve a target CTS value based on in-plane ($1/mL_c$) and through-plane (R_{eq}/R_{max}) design parameters.

We now have all the tools we need to calculate the physics-based coefficient of thermal spreading and enable robust prediction of system thermal design power.

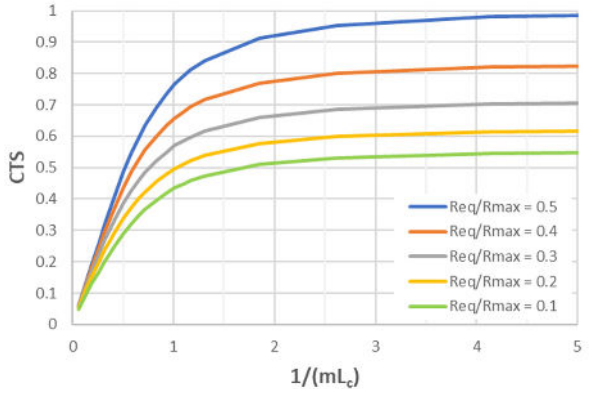

Figure 3 - Combined CTS as a function of in-plane and through-plane design parameters

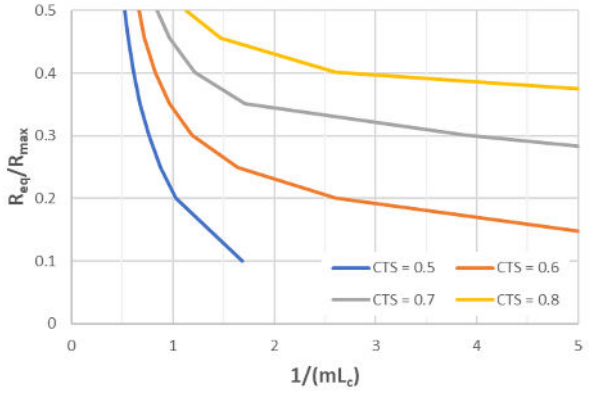

Figure 4 - In-plane and through-plane design parameters required to achieve desired CTS

Putting it into Practice

Let's demonstrate this for the notional device with the inputs specified in *Table 1*. It is common for the environment, temperature limits, and form factor to be known early in the design process.

INPUT	VALUE	UNITS
T_{limit}	45	°C
$T_{ambient}$	25	°C
h	10	W/m^2 - °C
L_c	75	mm
W	50	mm
$t_{housing}$	1	mm

Table 1 - Inputs for example calculation

Assuming we use a housing material construction with an effective thermal conductivity of 20 W/m-°C, the in-plane thermal performance is calculated in *Table 2*. The calculated fin efficiency is 0.55, meaning the device rejects heat from its top or bottom surface as effectively as an isothermal surface with 55% of the area.

PARAMETER	EQUATION	VALUE	UNITS
P	W + 2$t_{housing}$	52	mm
A_c	W$t_{housing}$	50	mm^2
k_{eff}	-	20	W/m-°C
m	Equation 3	22.8	1/m
1/mL_c	-	0.58	-
η	Equation 2	0.55	-

Table 2 - In-plane CTS calculation

The cross-section of the notional device is provided in *Figure 5*. Heat is assumed to be generated on the heat source located in the middle of the device. Heat leaving the front surface of the device passes through a thermal interface material (TIM) that is the same size as the heat source. Heat leaving the back of the device passes through the printed circuit board (PCB) and an air gap. The thickness (t) and thermal conductivity (k) of each layer is specified in *Figure 5*.

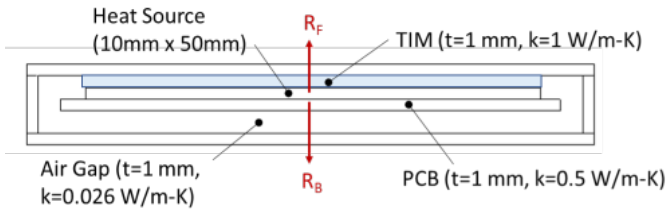

Figure 5 - Cross-section illustrating heat paths in a notional device

The thermal resistance in each individual layer is calculated using the one-dimensional resistance equation for heat conduction (*equation 4*). The resistance to the front and back of the device is calculated by combining the individual layer resistance values; this is achieved via a simple sum when the individual resistors are in series. The area used in the PCB and TIM resistance calculations is assumed to be that of the heat source (500 mm^2).

The resistance to the environment is calculated using the thermal resistance equation for heat convection. Note that the effective heat transfer coefficient (h) in this equation accounts for all heat rejection modes. In this example the value is based on the sum of an empirical correlation for natural convection and a linearized radiation heat transfer coefficient.

Table 2 summarizes the through-plane heat spreading calculation. The ratio of the equivalent resistance to the maximum resistance (R_{eq}/R_{max}) is 0.41. Given that this value is below 0.5, there exists an imbalance in heat transfer between the front and back surfaces of the device. The resulting through-plane multiplier ($M^*_{through\text{-}plane}$) is 0.85.

Now that we have calculated the in-plane and through-plane performance, we combine them in *Table 3* to calculate an overall

coefficient of thermal spreading of 0.47. The resulting thermal design power for the example device is thus 1.40 Watts. This is much lower than the ideal thermal design power of 3.00 Watts, illustrating the influence of in-plane and through-plane temperature gradients on device capability.

PARAMETER	EQUATION	VALUE	UNIT
R_{TIM}	$(t/kA)_{TIM}$	2.0	°C/W
R_{PCB}	$(t/kA)_{PCB}$	4.0	°C/W
R_{air}[1]	$(t/kA)_{AIR}$	13.4	°C/W
R_F	R_{TIM}	2.0	°C/W
R_B	$R_{PCB} + R_{AIR}$	17.4	°C/W
R_∞	1/hA	13.3	°C/W
R_{eq}	Equation 6	15.5	°C/W
R_{max}	Equation 7	37.7	°C/W
R_{eq}/R_{max}	-	0.41	-
$M^*_{thru\text{-}plane}$	Equation 5	0.84	-
[1] *Air gap conductions assumes lateral spreading can occur in PCB similar to the housing, 150mm x 50mm x η*			

Table 3 - Through-plane CTS calculation

If additional thermal capability is required, the thermal designer can iterate this process to converge on a more satisfactory set of design parameters. *Figure 4* can be used to guide the designer in determining the required in-plane and through-plane design parameters to achieve a satisfactory result.

PARAMETER	EQUATION	VALUE	UNIT
η	Equation 2	0.41	-
$M^*_{thru\text{-}plane}$	Equation 5	0.85	-
CTS	Equation 8	0.47	
TDP_{ideal}	Equation 1*	3.00	W
$TDP_{corrected}$	Equation 1	1.40	W
** Isothermal assumption, CTS = 1*			

Table 1 - Inputs for example calculation

Concluding Remarks

Thermal design power calculations provide powerful data for efficiently exploring the design space and making architectural decisions such as the form factor of the device, the targeted user experiences, material properties, device construction, and the supported thermal environments. A physics-based approach for calculating the thermal design power for a mobile phone or tablet is provided that includes the effects of both in-plane and through-plane thermal gradients. Approaches such as this are helpful when you don't have historical test data or are exploring new architectures. Additionally, the approach provides actionable data for reverse engineering the thermal requirements of the design to achieve a desired spreading coefficient or thermal design power.

While this method can be very useful, it does not replace detailed design and validation. It is instead intended to enable early design explorations before you transition to more detailed simulations and/or tests.

References

[1] Victor Chiriac, "A Figure of Merit for Smart Phone Thermal Management", Electronics Cooling Magazine, April 2017
[2] Frank Incropera and David DeWitt, Fundamentals of Heat and Mass Transfer, 4th Edition, Wiley (1996)
[3] Alex Ockfen, "Calculating Thermal Design Power for Mobile Consumer Electronics – Part 1", Electronics Cooling Magazine, February 2023
[4] Alex Ockfen, "Calculating Thermal Design Power for Mobile Consumer Electronics – Part 2", Electronics Cooling Magazine, August 2023

Revolutionizing Data Center Sustainability with Intelligent, Purpose-Built Solutions

Mukul Anand
Global Director of Business Development,
Applied HVAC Global Products, Johnson Controls

Introduction

By pairing an air-cooled, magnetic bearing chiller and mission-critical air handling units with the sophisticated AI capabilities of open source digital platforms, data centers can reduce energy use by allowing for a dynamic — rather than static — chilled water setpoint.

The primary objective for any data center is flawless data processing; critical to achieving that objective is high reliability and maximized uptime. However, to mitigate the effects of climate change, another attribute has become equally important — minimized environmental impact. Since maintaining uptime has traditionally required significant energy and resources, these goals seem to be at odds.

Data centers are one of the most energy-intensive types of buildings, consuming 10 to 50 times the energy per floor space of standard commercial office buildings and collectively using about 2% of the nation's total electricity consumption.[1] As technology leaders make significant net-zero and water commitments, they are seeking new innovations to reliably reduce energy and resource use.

Aside from the electricity that servers consume, HVAC equipment is responsible for as much as 40% of electricity use in data centers. To operate sustainably and profitably, it's critical these facilities optimize HVAC energy efficiency while ensuring data center uptime.

The latest innovations in HVAC and smart building technology make this outcome possible, cutting energy and water usage, carbon emissions and costs while ensuring the highest reliability. Mission-critical, computer room air handling units paired with an air-cooled, magnetic bearing chiller, digital solutions and building automation technology can significantly improve data center sustainability while maintaining an environment that supports reliability and uptime.

Maintaining Cold Aisle Temperatures

The temperature of the cold aisle determines how aggressively HVAC equipment and server fans must work, and therefore how much power they consume, to ensure the proper volume of air moves through servers to remove heat. A higher cold aisle temperature results in lower chiller power consumption. A lower cold aisle temperature results in a smaller volume of airflow being needed and less fan power consumption for the air handling unit fans and server fans.

To prevent hot spots in a data center's white space and ensure uptime, data center cooling strategies have historically favored lower cold aisle temperature and higher air flows — even beyond what's needed. This excess airflow acts as a buffer for an application that is close to the edge of the requirement. For example, if a certain server has higher than usual load on it, it may starve the cold aisle of cold air and may overheat. The extra airflow provides a safety net, but it also wastes energy.

[1] https://www.energy.gov/eere/buildings/data-centers-and-servers

Mukul Anand
With over 25 years of experience in the HVAC industry, I am a passionate and results-oriented leader who strives to deliver value-added solutions for data center customers worldwide. As the Global Director of Business Development at Johnson Controls, I leverage my expertise in datacenter cooling, product management, energy management, and applied HVAC to collaborate with our customers, understand their needs, and provide strategic guidance to reduce power consumption, water usage, and total cost of ownership. I am motivated by the mission of Johnson Controls to create a more sustainable and comfortable world, and I bring diverse perspectives and experiences to the team. In my current role, I lead the efforts to launch specialized products for the data center vertical, and partner with other business units to offer integrated solutions for fire detection, fire suppression, security, building automation, and controls.

Advances in server technology have made it possible for the latest generation of servers to operate at high ambient conditions in warmer cold aisles. Servers that can operate in a greater temperature range make it possible for a broader range of acceptable cold aisle temperatures.

By optimizing the cold aisle temperature, a data center can consume the minimum power required to cool it. Currently, this temperature is a static number. However, research into the effects of a dynamic cold aisle temperature proves that a dynamic cold aisle temperature can deliver optimum cooling according to the ambient conditions in the data center load at any given time – and the technology to do it is available now.

For instance, when it's very cold outside, there is an opportunity to use economization or free cooling and simultaneously lower the chilled water setpoint and lower the cold aisle temperatures. This reduces airflow and power consumption from the computer room air handler as well as server fans. When a data center uses a static chilled water setpoint and a static cold aisle temperature, this opportunity is lost.

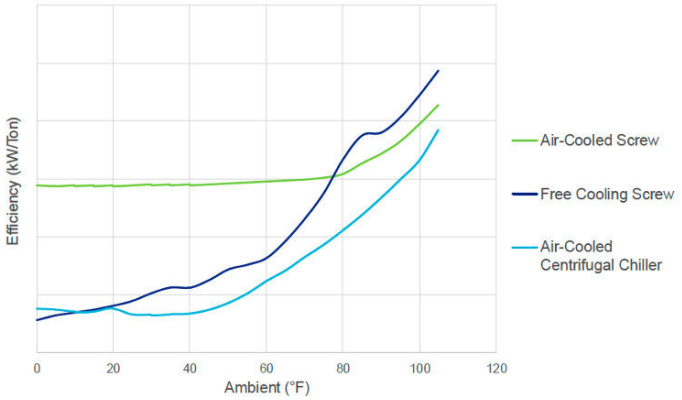

Figure 1 - showing power consumption of different efficiencies of chillers compared to cold aisle temperature

On the hottest afternoons of the year, the chiller power consumption is highest because the lift on the chiller is high. Chiller lift refers to the difference in pressure between the refrigerant in the condenser and the refrigerant in the evaporator. At higher lifts, the compressor consumes higher amounts of power to drive the thermodynamic cycle. The lift may be reduced by raising the chilled water setpoint and the cold aisle temperature for a few hours in the afternoon. This reduces the power consumption by the chiller compressor(s). The industry uses the term temporary excursion from ASHRAE Thermal Guidelines for Air Cooling of IT Equipment.

The pairing of an air-cooled, magnetic bearing centrifugal chiller and mission-critical, computer room air handlers with an open source digital platform and building automation system can drive cold aisle temperatures that suit data center loads at any given moment. A dynamic chilled water setpoint, and a dynamic cold aisle temperature overall, helps optimize a data center's power consumption without risking the uptime of the data center. This method of continuous optimization could lead to the best real-time energy efficiency of the data center while providing cold aisle temperatures that help maintain uptime.

Innovative Technology For an Evolving Industry

Historically, data centers have used chillers and other HVAC equipment that were designed for comfort cooling, not data centers. In comfort cooling, chilled water setpoints are around 44°F. However, server manufacturers are becoming more comfortable with processors and motherboards operating at higher temperatures, which means they can be cooled with chilled water upwards of 80°F.

Innovations in chillers for data center applications make it possible for chilled water setpoints to be anywhere from 70°F to 80°F, and sometimes even higher. This reduces power consumption and increases the number of annual hours, when free cooling can be used to significantly reduce the amount of power that is consumed by data centers throughout the year.

Designed specifically for data centers, air-cooled, magnetic bearing centrifugal chillers are optimized for increased temperatures inside the white space and the lifts that are prevalent in the data center industry today. They can deliver chilled water temperatures that are upwards of 80°F and cater to a low lift, resulting in greater energy efficiency.

While most data centers use air-cooled chillers that have free cooling coils to benefit from lower ambient conditions, air-cooled, magnetic bearing centrifugal chillers can operate at inverted conditions and provide free cooling without additional free cooling coils. Free cooling coils that are added to the condenser of the chiller can lead to inefficiencies and additional pressure drops, as well as heavier equipment and a larger carbon footprint. The weight they add to the chiller is embodied carbon, from the metal that makes up the coils, to heavier shipping and rigging weight, to the need for a building structure that inherently has more steel in it to support additional weight on the rooftop. Using a chiller that is lighter and provides inverted-operation free cooling positively impacts the carbon footprint of the building itself in many dimensions.

The friction-free, magnetic drive benefits uptime, as well. If power is interrupted, a typical chiller can take up to 10 minutes to restart. In comparison, magnetic bearing centrifugal chillers have much faster compressor restart times and can return to full load in as few as three minutes after power is restored. Because air-cooled, magnetic bearing centrifugal chillers use a variable-speed drive, there is no inrush current. This means a fast, controlled return to full capacity and setpoint.

To further improve data center sustainability, air-cooled, magnetic bearing chillers produce notably less sound than many screw chillers, and some use R-1234ze, a refrigerant with ultra-low global warming potential (GWP).

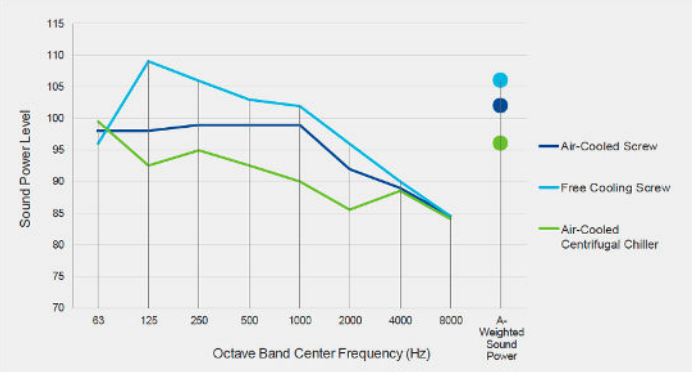

Figure 2 - showing sound levels of different types of chillers

When connected to an AI-based solution, air-cooled magnetic bearing centrifugal chillers combined with high-efficient mission-critical computer room air handlers designed with electronically commutated motors (ECM) can match cold aisle temperature with the real-time load and optimize energy use from moment to moment. Having a dynamic chilled water setpoint and cold aisle temperature optimizes energy use without risk to data center uptime.

Optimizing Energy Use Based on Real-Time Conditions

Intelligent digital services, like that provided by an artificial intelligence (AI)-based solution, integrated with air-cooled magnetic bearing centrifugal chillers and high-efficiency mission-critical computer room air handlers, provide the most optimized energy solution. Coupled with a dynamic water setpoint and a routine chilled water reset strategy offers even further energy savings. These solutions optimize airflow based on real-time conditions and can significantly reduce a data center's energy use.

As part of a digital platform, an AI-based solution can be either an advisory or a supervisory function sitting on top of the building management system (BMS). There, it ensures that data center personnel can evaluate the real-time data center loading and real-time data center requirements around the ambient conditions, as well as know the historical loading patterns or trends. Equipped with this valuable information, facility managers can ensure the system is operating as efficiently as it can.

A chilled water reset strategy can help reduce energy use during peak demand periods in data centers that experience high ambient temperatures. A chiller's power consumption depends on lift, and lower lift means less energy use. During the hottest afternoons of the year, a low chilled water temperature is required to cool the data center. To achieve this, lift and power consumption are typically high. However, the chilled water setpoint can be adjusted to a higher temperature for four or five hours in the afternoon to improve system energy efficiency while relying on a slight ramp-up of the high-efficiency ECM fans in the computer room air handlers.

This chilled water reset deviates from standard conditions and isn't permitted by some service-level agreements. To improve overall efficiency and data center sustainability, it's important to include chilled water reset for a set number of hours per year in service-level agreements.

Using historical trends, an intelligent cooling system can anticipate and prepare for the next loading change. For example, if a data center consistently generates a lot of heat around 8 a.m., the system can be automated to gradually ramp up capacity starting at 7 a.m. rather than running at 100% capacity at 7:59 a.m. This gradual ramp-up minimizes system spikes, improves energy efficiency and can even extend equipment life.

A combination of digital solutions, connected equipment and building automation technology can make data centers smarter and more sustainable. These solutions allow facility managers to continuously monitor equipment health and energy consumption in real time while automating key processes. Some solutions also offer easy-to-read dashboards that display trends and notify assigned personnel when set parameters deviate from assigned values. That allows facility teams to address issues, identify opportunities for energy savings and drive outcomes that matter most.

Improving Energy Efficiency and Uptime — Simultaneously

Technology leaders have very strict sustainability goals with aggressive deadlines to reach them. It's critical that data centers are equipped with innovative solutions to help achieve those goals as quickly as possible. Purposefully designed air-cooled, magnetic bearing centrifugal chillers combined with mission-critical, computer room air handlers driven by artificial intelligence can optimize sustainability according to real-world, white space conditions and significantly improve data center efficiency while maintaining uptime.

As servers become more capable of operating at high ambient conditions and data center owners and operators become more comfortable with warmer cold aisles, it's essential that HVAC equipment be ready to operate at higher chilled water setpoints and higher cold aisle temperatures. This shift in a long-held design mindset presents the opportunity to create a smarter, more sustainable data center architecture that collaborates and empowers overall energy efficiency and reliability. Air-cooled, magnetic bearing centrifugal chillers, mission-critical computer room air handlers and a logic-based BMS can grow and evolve with data centers, providing continuous improvement today and tomorrow.

Experimental Evaluation of Supercritical Carbon Dioxide as a Viable Coolant for Electronics Thermal Management

Wyatt Stottlemyre, Alec Nordlund, Joshua Gess
Enhanced Heat Transfer Laboratory, Oregon State University

Bharath Ramakrishnan, Husam Alissa
Microsoft Cloud Operations & Innovation Engineering

Wyatt Stottlemyre
Wyatt Stottlemyre currently works as a Thermal Hydraulic Engineer at Framatome in Richland, WA. In this role, he conducts analyses and design work for boiling water nuclear reactors. He obtained both his Bachelor's degree (BE) and Master's degree (MS) in Mechanical Engineering from Oregon State University. His prior research focused on heat transfer applications in various systems, including the development of a bio-inspired cooling skin patch, a supercritical carbon dioxide cooling loop and a hydraulic line for nuclear testing applications.

Alec Nordlund
Alec Nordlund is an Oregon State Graduate working in the Enhanced Heat Transfer Laboratory (EHTL). He began work under Dr. Joshua Gess in the EHTL during his sophomore year. Over the years his range of research has included cryogenic cooling of computer components, the use of high-pressure CO2 as a green refrigerant, and boiling heat transfer for data center cooling. He is now a faculty researcher focusing on improving the energy efficiency of data centers through immersion cooling and other novel approaches.

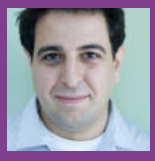

Bharath Ramakrishnan
Bharath Ramakrishnan is currently a Sr Mechanical Engineer working with the Microsoft CO&I's Research and Advanced Development (RAD) Team at Redmond, WA, USA. His research background is on data center thermal management with an emphasis on all forms of high-density liquid cooling techniques. At a micro level, his recent research interests are into exploring microfluidic cooling technologies and advanced direct to chip cooling for next generation IC packages. At a macrolevel, his latest interests are into developing data center waste heat recovery and direct air capture (DAC) systems.

Bharath Ramakrishnan received his Bachelor's degree (BE) in Mechanical engineering from CIT, Coimbatore, India in 2010, Master's degree (MS) in Mechanical Engineering from Auburn University, Auburn, AL, USA, in 2014, and the Ph.D. degree in Mechanical Engineering from Binghamton University, Binghamton, NY, USA, in 2019.

Husam Alissa
Husam Alissa is the Director of the Systems Technology Team in Microsoft's Research and Development group/ CO+I CTO Office. His focus area is on systems & vertical integration technology initiatives involving sw-chip-server-datacenter. This includes cooling (air, direct to chip, immersion, and cryogenics), performance, architecture, reliability, efficiency, sustainability/LCA, and TCO, with more than a hundred publications and filed patents on these topics. Husam's work has received many recognitions including DCD Award for Mission Critical Tech Innovation, IEEE Micro Top Picks, IEEE TCPMT Best Paper Award, ASME InterPACK Outstanding Paper Award, NewYork State Assembly Early Career Achievement Award, and S3IP Distinguished Doctorate Dissertation Award. He is a member of IEEE, ASHRAE TC9.9, ASME, OpenCompute, & iMasons.

Dr. Joshua Gess
Joshua Gess received his PhD from Auburn University in Mechanical Engineering in 2015 and his B.E. in Mechanical Engineering from Vanderbilt University in 2005. Prior to receiving his PhD, he spent six years in the defense industry at Northrop Grumman in Madison, AL designing mobile command centers for Army, Navy, Marines, and National Guard customers. His research is focused on energy-dense electronics thermal management and fundamental multiphase heat transfer. He developed a two-phase Particle Image Velocimetry (PIV) technique to calculate net coolant flow rates to boiling surfaces and was the 2015 MVP of the Auburn Tigers Wheelchair Basketball Team.

Introduction

In the development of modern-day thermal management systems, we are continuously looking to implement coolants that offer high heat transfer performance, low pumping power requirements, are cost-effective and have a low environmental impact. Supercritical carbon dioxide (SCO2) has a range of incredible properties that lend it to meeting all these needs, even contending with conventional liquid-vapor phase change fluids that are actively cooling our high-demand electronic systems. The fluid does not experience critical heat flux conditions and has a relatively low operational temperature, at just over 31°C. Carbon dioxide is also a non-explosive, non-flammable, non-toxic fluid that is highly accessible and cost-effective. Admittedly, SCO2's high operational pressure and heat rejection temperature requirements can pose design challenges that must be accounted for. However, SCO2 has already been integrated as an active fluid into a range of high-efficiency power cycles with promising results [1,2].

Characteristics of Supercritical Carbon Dioxide

Carbon dioxide becomes supercritical when conditioned beyond critical point properties (31.1°C and 78.3 atm). At this state, the fluid experiences spikes in specific heat capacity that rival or exceed traditional phase change fluids, while operating at lower, gas-like densities. *Figure 1* illustrates the specific heat magnitudes that can be achieved and the operational temperature envelopes that accompany them.

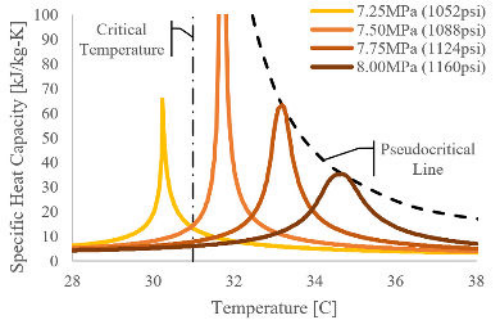

Figure 1 - Carbon dioxide specific heat capacity versus temperature plot at both subcritical (left) and supercritical pressures.

At subcritical pressures, specific heat capacity values spike at the saturation temperature, whereas at supercritical pressures they spike at the pseudocritical line. It is at this line - where the fluid transitions from a liquid-like to a gas-like state upon the absorption of heat –at which we want our systems to operate in order to maximize performance. Unlike the mechanisms behind conventional phase change, this process does not result in the generation of visible nucleation sites or bubbles. Instead, the fluid becomes less dense and consequentially easier to move. The combination of higher specific heat capacities and gas-like fluid density gives SCO2 the ability to effectively cool high heat flux components with lower pumping power requirements than many alternative phase-change systems.

This study is a direct continuation of the work performed by the Enhanced Heat Transfer Laboratory at Oregon State University (OSU) in 2019, where the first SCO2 cold plate made with additive manufacturing techniques was evaluated. The conclusions drawn from that study, in comparison to other industry-standard coolants, distinguished SCO2 as a highly competitive coolant for electronics cooling applications [3,4]. The experimental design of the present work aims to simulate a data center environment such that the results more closely reflect real-world applications.

Experimental Facility

A carbon dioxide conditioning loop, in conjunction with a heated experimental fixture, was constructed to generate and evaluate the performance of SCO2 in an electronics cooling application. The conditioning loop serves to pressurize and heat saturated CO2 (out of the cylinder) to the desired supercritical state. The heated experimental fixture is comprised of a pure copper block, surrounded by three inches of insulating Teflon™ and supplied with power by four cartridge heaters. A custom aluminum cold plate is bonded to an exposed copper surface that acts a hot processor chip surrogate.

The cold plate itself, which can be seen in *Figure 2*, was manufactured with direct metal laser melting techniques. Internally, it is comprised of seven parallel channels with hydraulic diameters of just over a millimeter and seven circular thru-holes, which are visible at the base. These holes are essential for the temperature-sensing technique utilized in this study. Geometric parameters and manufacturing tolerances of interest were verified using neutron radiography techniques at OSU's TRIGA reactor.

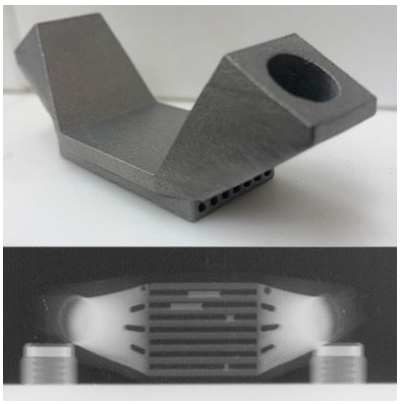

Figure 2 - Additively manufactured aluminum cold plate to evaluate SCO2 performance. Isometric (top) and neutron radiography views (bottom) provided.

While most of the sensing techniques used to capture data were fairly standard, one requiring further explanation is the fiber optic temperature sensor used to collect cold plate wall temperature values. By use of the phenomenon known as Optical Backscattering Reflectometry (OBR), this sensor is able to generate numerous, discrete temperature measurements along the length of a fiber optic cable. By routing this cable (back and forth) through the base of the cold plate, we are able to generate two-dimension-

al temperature maps that reflect the thermal performance of the coolant, as illustrated in *Figure 3*.

OBR utilizes Rayleigh backscattering techniques to pinpoint the location of the fiber optic cable relative to its Teflon sheathing. Light signal reflection times generate a baseline reading, and as the sheathing changes form under the application of heat and thermal expansion, the change in light reflection times may be correlated to changes in local strain and temperature. In our case, this allows for the collection of internal temperature measurements from within the cold plate wall and a deeper understanding of local heat effects at a frequency of 10 Hz [5].

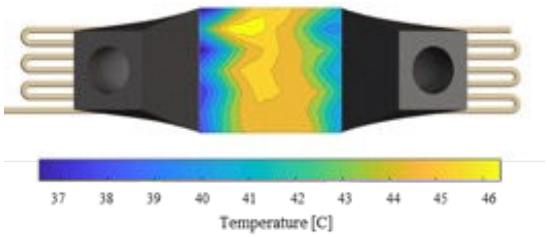

Figure 3 - Sample temperature map generated by OBR fiber optic sensor with a resolution of 1.3mm.

Generating these temperature maps is essential to evaluating a given system's local thermal management needs. Beyond the ability to visualize the streamwise temperature distribution of the cold plate itself, we are also able to see the exact location of localized hotspots and their magnitudes. Furthermore, these discrete wall temperatures can be used to compute local heat transfer coefficient values, which can be very powerful in evaluating performance and working towards system optimization. From this information, adjustments can be made such that the desired inlet fluid temperature and corresponding span are adjusted to provide the highest cooling capabilities to the regions of the heated surfaces that need it the most.

Evaluation of Performance

In conjunction with the experimental data captured, numerical models were generated for convective heat transfer coefficient (HTC) and cold plate pressure drop data sets. All of the data presented within this section were taken at a constant pressure of 7.93MPa (1150 psi), mass flow rate (500g/min), and input power delivered by the cartridge heaters (200W) – translating to a heat flux density of 41W/cm^2.

Figure 4 illustrates the relationship between the system's average HTC and temperature. Here, it can be seen that maximum HTC values of around 19kW/m^2-K are measured at around 33.5°C – in close proximity to the expected pseudocritical temperature of 34.2°C. HTC values are also generally higher when the fluid is at lower temperatures (liquid-like) and begin to drop off as the fluid becomes increasingly gas-like. While there is an apparent disconnect between the numerical model and experimental data, it should be noted that the model captures the general trends of the experimental data – and even reflects comparable HTC values around the pseudocritical temperature, which would likely be the target operational point set by designers.

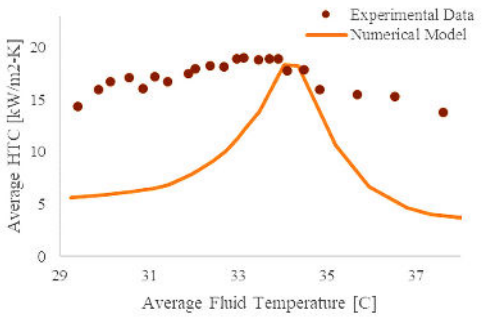

Figure 4 - Average heat transfer coefficient with respect to SCO2 fluid temperature, reflected both experimentally and by the numerical model.

Experimental HTC values were computed using Newton's Law of Cooling, assuming a uniform heat flux. Local wall temperatures are reflected by the OBR temperature measurements, while the fluid temperature was computed using calibrated thermocouples in the flow stream at the cold plate's inlet and outlet. The heat transfer area used in this calculation reflect the area of the channels themselves (with the exception of the top surface).

$$HTC_x = \frac{q_x}{A_x(T_{w,x} - T_{f,x})}$$

While all of the local wall temperatures could be directly measured through the fiber optic sensor, only the inlet and outlet fluid temperatures were experimentally measured. An energy balance on the fluid was utilized to compute average local fluid temperature values from within the cold plate, with the outlet temperature bounded by the experimental reading.

$$T_{f,x+1} = T_{f,x} + \frac{q_x}{\dot{m}c_{p,x}}$$

Numerically modelled HTC values were computed by use of a flow boiling correlation, which was adapted for supercritical fluid use by altering the thermodynamic quality and saturation properties accordingly [6]. Here, the single-phase HTC values were computed using the Dittus-Boelter equation. The supercritical HTC values (SC) were computed by multiplying the computed single-phase HTC (SP) by two constants – which incorporate a ratio of the fluid densities at effective "supercritical" saturation temperatures, a supercritical quality and a specific enthalpy term with the Froude number assumed to be unity as well as the surface–fluid combination value ($G_{s,f}$).

$$HTC_{SC} = HTC_{SP}(C_1 + C_2)$$

where

$$C_1 = 0.6683\left(\frac{\rho_l}{\rho_v}\right)^{0.1} \underline{X}^{0.16}(1-\underline{X})^{0.64} f(Fr)$$

$$C_2 = 1058\left(\frac{q_s^{"}}{\dot{m}^{"} h_{fg}}\right)^{0.7} (1-\underline{X})^{0.8} G_{s,f}$$

Figure 5 shows how the local HTC varies in the streamwise direction of the cold plate, also using the above equations. Here it can be seen that the experimentally generated HTC values experience very little change, whereas the numerical model predicts more variation. This is likely due to the uniform heat flux assumption that had to be made without the implementation of a thermal test vehicle (TTV). Nonetheless, the streamwise model again comes close to predicting HTC values near the pseudocritical temperature. Knowledge of the local heat flux distribution would likely close this gap and give more merit to the numerical model.

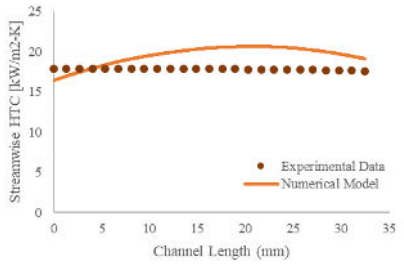

Figure 5 - Streamwise heat transfer coefficient plot generated at a fluid inlet temperature of 34°C, reflected both experimentally and by numerical model.

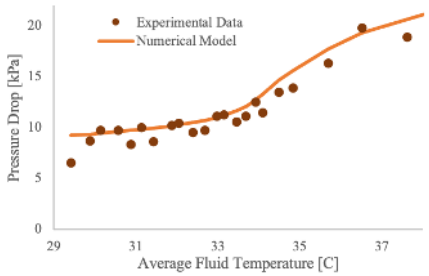

Figure 6 - Cold plate pressure drop with respect to average SCO2 fluid temperature, reflected both experimentally and by the numerical model.

Figure 6 demonstrates the relationship between cold plate pressure drop and average fluid temperature. As the fluid heats up, the Reynolds number increases due to thermodynamic fluid property changes, driving up friction factor values and therefore pressure drop values. The inflection point, again near the pseudocritical temperature, is indicative of favorable operational temperatures.

Experimental values were collected by use of a high-accuracy differential pressure sensor and modeled values were generated through the Darcy-Weisbach equation in conjunction with the Colebrook equation.

$$\Delta P = f\frac{\rho v^2 L}{2D_H}$$

where

$$\frac{1}{\sqrt{f}} = -2.0log\left[\frac{e/D_H}{3.7} + \frac{2.51}{Re_D\sqrt{f}}\right]$$

Temperature sweeps were conducted to evaluate optimal SCO2 operational temperatures for the given fluid pressure. From the data presented, an operational temperature range of around 33-34°C produced the highest HTCs with reasonably small pressure drops and therefore lower pumping power requirements.

Conclusions

When pressurized to 7.93MPa (1150psi) and flowing at only 500g/min (1SLPM), SCO2 was able to produce HTCs nearing 20kW/m²-K, dissipating heat flux densities of 41W/cm² within a relatively simple cold plate that had just seven parallel channels and exhibited no sign of a critical heat flux condition. At the same operational parameters, a pressure drop of only 12kPa was measured; requiring only 0.1% of the input power to pump the fluid through the cold plate. In conjunction with SCO2's low environmental impact and abundance, this study is indicative of the fluid's potential as a highly competitive coolant in electronics cooling applications. It is also important to mention that operation at pressures nearer to the critical point and geometric optimization could substantially improve upon the metrics displayed here. It is expected that the numerical models generated for this study, while able to produce experimentally comparable values, would have a better agreement if the local heat flux density was known, thereby warranting future studies.

References

[1] Weiland, N. T., R. A. Dennis, S. Lawson, and P. Strakey. 2017. Fundamentals and applications of supercritical carbon dioxide (sCO2) based power cycles. (K. Brun, P. Friedman, and R. Dennis, eds.). Oxford Woodhead Publishing.

[2] Marion, J. 2022. "Supercritical CO2 10 MW Demonstration Project Under Construction." Turbomachinery International, 2022.

[3] A. Nordlund, M. Harrison, B. Fronk, J. Gess, 2019, "Operation of a Supercritical CO2 Cold Plate for Electronics Cooling Applications" Thermal Technologies Workshop, Redmond WA

[4] B. Ramakrishnan et al., "CPU Overclocking: A Performance Assessment of Air, Cold Plates, and Two-Phase Immersion Cooling," in IEEE Transactions on Components, Packaging and Manufacturing Technology, vol. 11, no. 10, pp. 1703-1715, Oct. 2021, doi: 10.1109/TCPMT.2021.3106026.

[5] Optical Backscatter Reflectometry (OBR) Overview and Applications Introduction Reflectance and Return Loss Measuring Return Loss. n.d. Accessed: May. 17, 2023, https://www.lunainc.com/sites/default/files/assets/files/resource-library/OBR%20-%20Overview%20and%20Applications.pdf

[6] Kandlikar, S. G., J, Heat Transfer, 112, 219, 1990.

Machines Now Fill and Perceive Scenes for Scientists and Engineers

Nhi Quach, Youngjoon Suh, Jewoo Park,
University of California, Irvine

Yoonjin Won
Stanford University

Introduction

Artificial intelligence (AI) has emerged as a powerful tool empowering scientists and engineers to interact with computers in innovative ways, thereby revolutionizing numerous fields. By leveraging AI, we can collaborate with machines to solve complex problems, gain valuable insights, and achieve significant advancements across diverse domains. One significant application of AI technology is deep learning-based computer vision for image processing. Computer vision's primary objective is to enable machines to interpret and comprehend visual data. To describe a scene effectively, the traditional computer vision approach extracts informative patches from digital images through algorithms, such as threshold and edge detection. Deep learning, on the other hand, has emerged as a powerful paradigm in computer vision, revolutionizing how machines process visual information. Deep learning models, particularly convolutional neural networks (CNNs), autonomously learn salient features directly from images. Instead of relying on explicit programming and hand-engineered rules, CNNs are trained on vast amounts of labeled data to automatically discover relevant patterns and structures within images. The advancements have led to great leaps in performance for visual tasks such as image segmentation, classification, object detection and track-

Nhi Quach
Nhi Quach is a Materials Science and Engineering Ph.D student at the University of California, Irvine who's research focus is on material coating effects on transport properties. Her aim is to provide understanding of liquid kinetics within porous materials to optimize transport phenomena for heat transfer or mass transfer applications. Her work has been recognized in the Nasser Grayeli Outstanding Student Poster Award at ASME's interPACK 2020.

Jewoo Park
Jewoo Park is a visiting researcher at the University of California, Irvine in the Department of Mechanical and Aerospace Engineering. His research topic is the reliability and durability of self-driving autonomous vehicles. He has 15 years of experience at the world-renowned vehicle company and is one of the group of ISO 26262 experts on Camera, Radar, and LiDAR sensor testing. He is an expert in developing sensor test modules and scenarios, with the focus being deterioration of sensor performance and physical deformation.

Youngjoon Suh
Youngjoon Suh is a postdoc at the University of California, Irvine in the Department of Mechanical and Aerospace Engineering. The overarching aim of his research aims to gain fundamental insights into two-phase transport physics by linking surface design, real-time nucleation statistics, and heat and mass transfer performances. His main research thrust models the interconnected relationships among boiling/condensation surfaces, bubble/droplet statistics, and heat transfer performance by integrating experimental metrology, and machine learning. His work has been featured in the covers of various high-impact journals including Small, Journal of Colloid and Interface Science, and Advanced Science. He is also a recipient of the student keynote award at μFIP 2021 and 2022, the best poster award at ICNMM 2019, and the 2018-2019 UCMexus Small Grant Award.

Yoonjin Won
Yoonjin Won received the Ph.D. degree in Mechanical Engineering from Stanford University. She is currently an Associate Professor of Mechanical and Aerospace Engineering at the University of California, Irvine, USA, where her group studies thermofluidic and interfacial phenomena by integrating novel metrology, computer vision, scientific machine learning, and data. Dr. Won was a recipient of the National Science Foundation CAREER Award, ASME Early Career Award, ASME Women Engineer Award, ICNMM Outstanding Leadership Award, and the Emerging Innovation/Early Career Innovator from UCI Beall Innovation Center. Her research has been recognized through invited presentations at GRC, MRS, ICNMM, mTAS, microfip, ASTFE TEC Talk, NISE, and best paper awards at InterPACK, ITHERM, ICNMM, NSF-JST, and other places.

ing, and restoration. These capabilities have become accessible to the public over the past decade. The ability of machines to accurately analyze and comprehend visual information has the potential to transform our daily lives, advance scientific understanding, and revolutionize various real-life applications, as illustrated in *Figure 1*.

Firstly, deep learning-based computer vision seamlessly integrates into various scientific research fields in *Figure 2*. One of the main challenges for scientists and engineers has been the capability to interpret scientific data and extract meaningful features from their experiments. The ability of machines to differentiate, harvest, and infer information from images opens new research avenues for researchers to study what has been deemed impossible before. For instance, in the biomedical and healthcare sector, computer vision models are now helping medical physicians

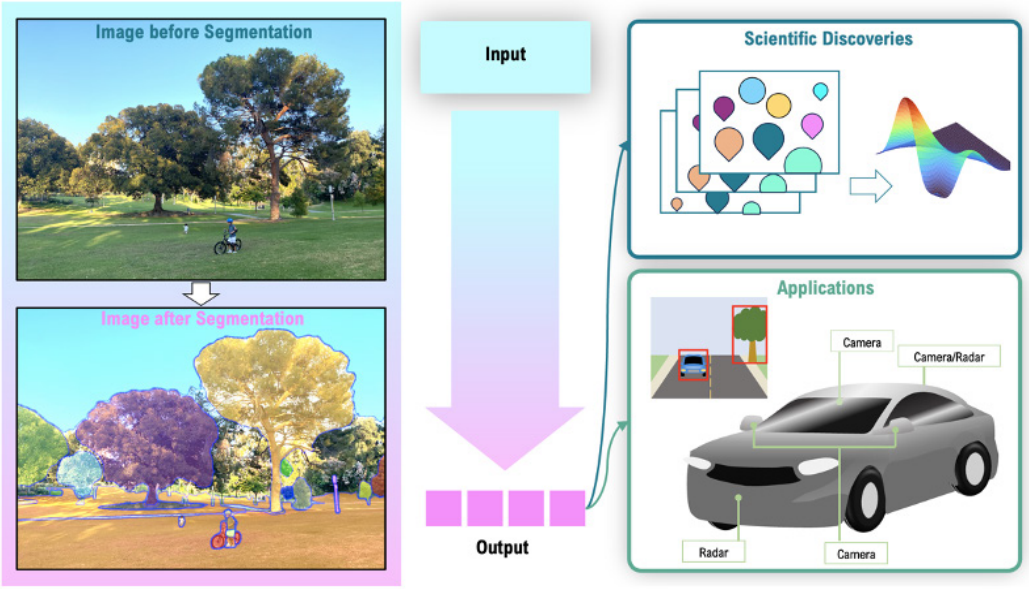

Figure 1 - Digitalizing visual scenes at the University of California, Irvine through deep learning-based computer vision (Segment Anything), categorizing objects into people, trees, bikes, and sky. These capabilities are poised to advance scientific discoveries and enable new engineering applications.

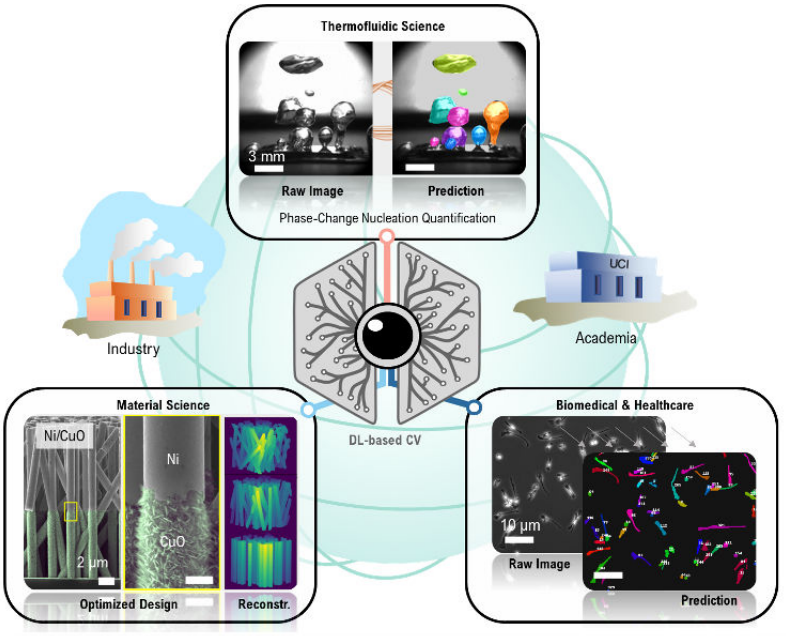

Figure 2 - Deep learning-based computer vision can assist with interpretating scientific data into features, such as thermofluidic bubbles, biology cells [1-3], or optimizing the design of materials [7].

make complex diagnostics spanning dermatology, radiology, ophthalmology, and pathology by offering second opinions and detecting anomalies within medical images.

The thermofluidic science community can also tackle century-old problems using modern techniques, such as deep learning-assisted computer vision [1-3]. While phase change processes can create phase boundaries in the forms of bubbles and droplets, the access to these feature statistics can aid researchers in revisiting and building mechanistic models after high-speed videography. The training nature of deep learning-based computer vision models expands the usage applicability to a broad range of other visualization data, such as videography with low resolutions, fluorescence microscopy, and even infrared (IR) imaging. The ability to extract and record physically meaningful features from visual scenes has tremendous implications for real-time monitoring and dynamic analysis of complex behaviors [2, 3], screening and anomaly detection [4-5], and the prediction and forecasting of certain events, such as boiling crisis or dryout [1, 6]. The collaborative information, along with optimization models, can be used to inversely design cooling structures, such as fins, pillar, or channels, for better performance even with a minimum number of experiments [7]. The evidence is clear that computer vision offers tremendous advantages for researchers across various fields. The extent to which such technologies will translate into positive impacts on society depends on how actively they are adopted and explored in various scientific fields.

In addition to scientific research, various successes have been achieved in employing computer vision for real-life applications, such as in autonomous robots or vehicles. [9]. Autonomous robots include delivery drones for fast package transport or search robots for locating people during disaster or collecting information at other planets. Once again, visual information from various sensors plays a critical role in assisting with applications. In this process, it is imperative to collect high-quality visual information. However, the process faces numerous challenges arising from external factors, such as fog, rain, dust, and bugs, and internal factors, such as temperature and thermal cycling, as demonstrated in *Figure 3*. For instance, condensed droplets or frost on the camera lens obstruct the physical view during image collection. Moreover, the distribution of rain or fog droplets affects the quality of visual data captured by sensors like LiDAR due to scattering effects on transmission wavelengths. Therefore, it becomes crucial to understand various influencing factors and their impact on the visual information and performances.

Addressing concerns about the impact of various influencing factors on optical measurements can involve either hardware or software solutions. Mechanical or materials scientists have developed hardware solutions to be incorporated and researched to remove debris and buildup on optical lenses. External camera lenses are coated with hydrophobic materials to prevent condensation and further frosting. Or lenses are installed with cleaners that involve a high-pressure spray system with a small amount of water. There are also research directions involving electrostatic and pulse heating, which can prevent or delay particle attachment or droplet formation on the surface. While hardware solutions have been developed for a long time, software solutions

Figure 3 - Computer vision challenges and difficulties shown with declining classification count and accuracy when comparing images taken from a clear lens (left) to images from a droplet covered lens (right).

are gaining popularity due to recent developments in deep learning-based computer vision technology. Post-processing through software solutions has led to an exploration of image restoration or reconstruction, a technique used to remove artifacts from a corrupted image to a clean image. The conventional approach to image restoration involves filling in missing or affected regions with information from surrounding pixels. However, this method, known as inpainting, was limited by the available information in the image. When dealing with large-affected areas, the surrounding pixels may not provide sufficient data to restore the missing sections effectively.

Recent advancements in deep learning methods have helped address the issue of insufficient pixel information in image restoration. These methods typically involve the use of encoder-decoder neural networks. Training datasets for these networks consist of pairs of corrupted images and their corresponding ground-truth images. The encoders are responsible for identifying the image features that require restoration, while the decoders work to recover the image quality during training. Consequently, machine learning models such as generative AI or generative adversarial networks (GANs) are now emerging as promising candidates for addressing computer-vision-related limitations [8-12]. GANs have the benefit of generating discrimination between behaviors. GANs aim to emulate human brain characteristics and generate outputs consisting of two sets of convolution layers simultaneously trained with a generator and a discriminator. The generator's role is to produce authentic-looking images, while the discriminator's task is to differentiate between real and generated ones. In scenarios where artifacts are present, the generator employs an attentive-recurrent network assigning higher values and weights to focus on corrupt regions during training. Through numerous epochs of training, the recurrent features are emphasized, creating an accurate mask that highlights the region needing restoration. The iterative process continues until the discriminator can no longer distinguish the fake images generated by the generator from real images, thereby signifying the completion of the restoration process.

The GAN's restoration capability can also improve the capability of object segmentation and classification even with environmental artifacts, in this case, droplets, as shown in *Figure 4* [8], which is essential for autonomous robots or vehicles. Here, the images are captured when the droplets are sprayed on the optical camera. The sprayed droplets are segmented and quantified by counting the number of pixels above a threshold of 50, resulting in four levels of increasing artifact severity: 1, 2, 3, and 4. The samples are thereby labeled as 1, 2, 3, and 4 accordingly. For the evaluation,

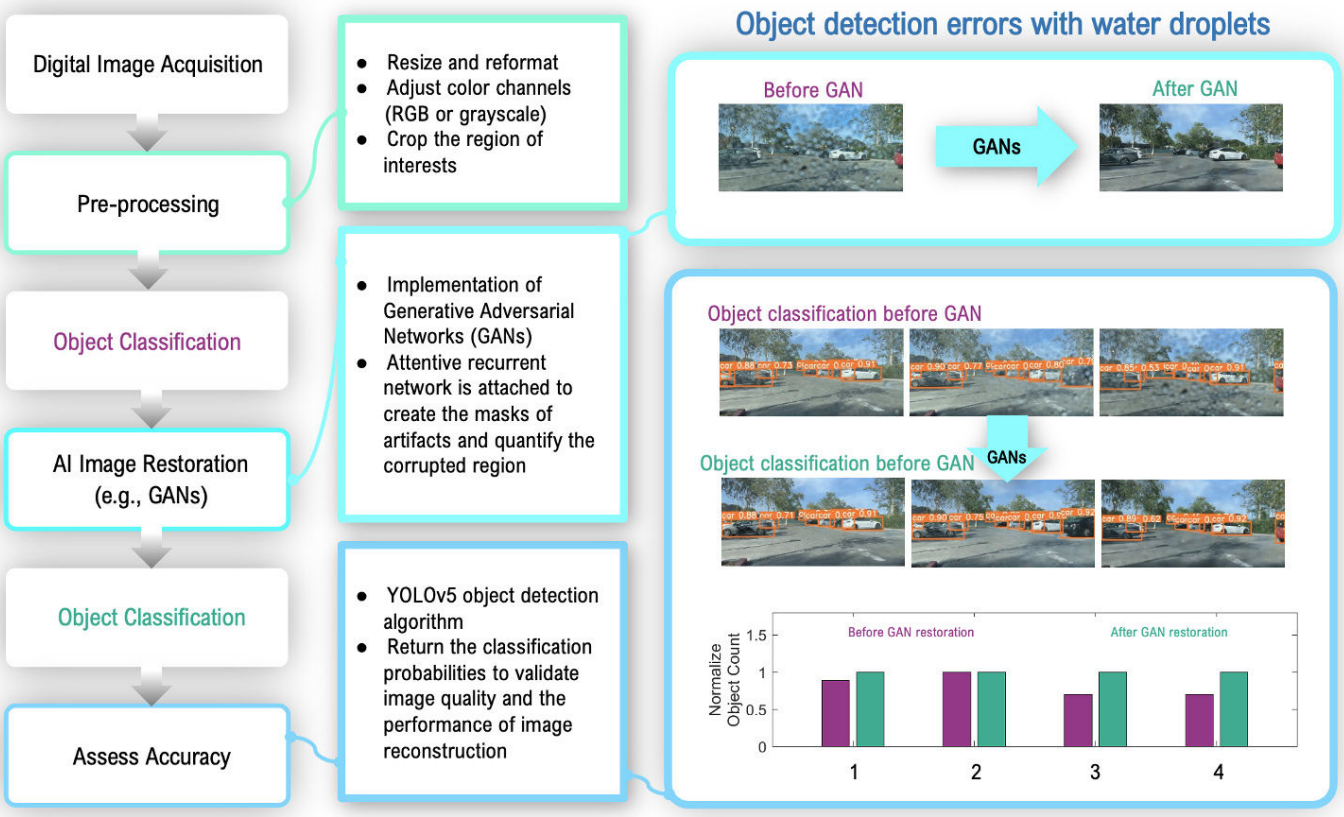

Figure 4 - Flow chart detailing the processing for image restoration and comparison of the number of objects counted with YOLOv5 before (purple) and after the GAN restoration (green).

the images are segmented by using computer vision algorithms to count the number of objects of interest (e.g., cars). Subsequently, the restored images after applying GAN are analyzed. *Figure 4* showcases the images before and after GAN restoration. The plot (right bottom) indicates that the number of classified objects increases by 30%, and the probability of classification increases by 10% after GANs restoration. These findings confirm the potential of GAN and deep learning-based computer vision models for real-world scenarios, especially in mild weather conditions.

This GANs' restoration capability can also contribute to data interpretation. Researchers often face challenges in obtaining high-quality data, especially when conducting experiments involving high-speed videography, as is the case in processes like boiling and condensation, which involve rapid nucleation and departure activities. It's crucial to emphasize that GANs not only excel at eliminating unwanted artifacts and repairing corrupted image segments but also possess the potential to offer intuitive, high-speed screening and analysis capabilities for rapidly evolving and intricate processes through automated object deblurring. Consequently, the integration of such deep learning-based computer vision applications holds the potential for practical improvements in enabling high-quality video analysis or screening, even with non-laboratory-grade cameras.

Despite all the promising aspects of machine learning, it's important to recognize that deep learning models come with inherent costs. Developing robust models requires the use of extensive datasets and multiple training iterations. For example, in a recent paper focused on scientific discoveries related to bubbles and droplets, a minimum of 2,500 images were used for training and testing the deep learning models [4], even with a ResNet backbone. It's worth noting that such ResNet backbones are often pre-trained on millions of images from the ImageNet database, enabling the pretrained network to classify images into 1,000 object categories. This emphasizes the importance of utilizing pretrained networks that can cover diverse domains, substantially reducing the computational demands of model training.

Acknowledgements

We want to acknowledge the support and funding provided by the Office of Naval Research (ONR) and the National Science Foundation (NSF). We would like to extend our gratitude to Annie Dinh & Liu Laboratory, Chuanning Zhao, Ruey-Hwa Cheng, and Miri Chen for their valuable contributions to the image data used in this study.

References

[1] *Y. Suh, R. Bostanabad, and Y. Won. "Deep learning predicts boiling heat transfer." Scientific reports, 11.1, 1-10, 2021.*

[2] *Y. Suh, et al. "A deep learning perspective on dropwise condensation." Advanced Science, 8.22, 2101794, 2021.*

[3] *J. Lee, Y. Suh, M. Kaciej, P. Simadiris, M. T. Barako, and Y. Won. "Computer vision-assisted investigation of boiling heat transfer on segmented nanowires with vertical wettability." Nanoscale, 14.36, 13078-13089, 2022.*

[4] *K-H. Yu, A.L. Beam, and I. S. Kohane. "Artificial intelligence in healthcare." Nature biomedical engineering, 2.10, 719-731, 2018.*

[5] *C. Zhao, J. T. Eweis-Labolle, R. Bostanabad, and Y. Won, "Inverse Engineering of Spatially Varying Micropillars for Heterogenous Heat Map," presented at Third Conference on Micro Flow and Interfacial Phenomena (μFIP), June 2023, Evanston, IL, USA.*

[6] X. Dong, et al. "Microscopic image deblurring by a generative adversarial network for 2d nanomaterials: implications for wafer-scale semiconductor characterization." ACS Applied Nano Materials, 5.9, 12855-12864, 2022.

[7] A. Rokoni, L. Zhang, T. Soori, H. Hu, T. Wu, and Y. Sun. "Learning new physical descriptors from reduced-order analysis of bubble dynamics in boiling heat transfer." International J. Heat and Mass Transfer, 186, 122501, 2022.

[8] Y. Suh, P. Simadiris, S.H. Chang, and Y. Won, "In micro Flow and Interfacial Phenomena," presented at MicroFIP, Irvine, 2022.

[9] D. Floreano and R. J. Wood. "Science, technology and the future of small autonomous drones." Nature, 521, 460-466, 2015.

[10] Z. Xiong, W. Li, Q. Han, and Z. Cai. "Privacy-Preserving Auto-Driving: A GAN-Based Approach to Protect Vehicular Camera Data," presented at 2019 IEEE International Conference on Data Mining (ICDM), Beijing, China 668-677, 2019.

[11] N. V. Quach, et al. "Machine Learning Enables Autonomous Vehicles under Extreme Environmental Conditions," presented at 2022 ASME interpack, Garden Grove, CA, USA, 2022.

[12] J. Zhang, H. Chen, and Z. Wang. "Droplet Image Reconstruction Based on Generative Adversarial Network." J. Phys. Conf. Ser., 2216, 012096, 2022.

[13] R. Singh, R. Garg, N. S. Patel, and M. W. Braun. "Generative Adversarial Networks for Synthetic Defect Generation in Assembly and Test Manufacturing." Asmc Proc, 9185242, 2020.

[14] Y. Suh, et al. "VISION-iT: Deep Nuclei Tracking Framework for Digitalizing Bubbles and Droplets." Available at SSRN 4491956, 2023.

[15] S. Chang, et al. "BubbleMask: Autonomous visualization of digital flow bubbles for predicting critical heat flux." International Journal of Heat and Mass Transfer, 217, 2023.


Call for Authors
and Contributors!
Want to be a part of the next issue of Electronics Cooling? Have an article or blog post you'd like to write for Electronics-Cooling.com?
Let us know at
editor@electronics-cooling.com
electronics COOLING
www.Electronics-Cooling.com

Bad Data!

Ross Wilcoxon
Associate Technical Editor for *Electronics Cooling*
Collins Aerospace

Overview

Sometimes, regardless of how carefully we conduct testing to gather data, we end up with results that just seem wrong. This could be a sign that we have stumbled upon an earth-shattering breakthrough that will change the world's understanding of fundamental physics[1]…. or, it's possible that a mistake in the testing led to bad data. This column will discuss a few examples of ways that testing mistakes that led to the collection of data that didn't exactly tell the correct story.

One potential source of bad data is if there is a selection bias in the process of collecting data. This occurs when the method of collecting data tends to have a bias that slightly shifts the distribution of the collected data to one side of the normal distribution of the population. Classic examples of this have been seen in political polling conducted with landline telephones: telephone-based polls in 1936 had a bias to more wealthy voters while the same method in 2020 resulted in a bias to older voters. One of the challenges in thermal testing is to ensure that the physics of temperature measurement methods don't introduce a bias in the results. Thermocouple measurements tend to generally be low, particularly when large thermocouple wires that can act as cooling fins are used. When exposed to long-term high temperatures, thermocouple drift could influence results in testing conducted over long periods of time. Accurate infrared temperature measurements rely on knowing something about the emissivity of the surface being measured – if that emissivity is not uniform or changes over time, bad data can be the result.

While knowledge of basic statistical approaches is important for data analysis, a healthy dose of skepticism is also helpful. Data are collected by human beings, who are known to occasionally make mistakes. When faced with data that look strange, it is a good idea to take the advice of the disembodied TSA voice at the airport: if you see something, say something. The strange results may in fact be accurate – but it is often worth the effort to double-check that the data haven't been biased by a measurement error.

A few years ago, I was asked to analyze data collected in a study to evaluate the impact of solder voids on the solder joint reliability of ball grid array (BGA) components subjected to thermal cycling. For this testing, 15 test boards were assembled with three different-sized daisy-chain BGA components with different configurations of microvias in the solder pads on the test board. The 'BGA56' was a 6mm x 6mm BGA with 56 solder balls on a 0.5mm pitch. Each test board included 4 replicates of the BGA56 with microvias in the test board solder pads (reference designators U1, U11, U15 and U24 correspond to the four locations where they were placed on the circuit board). Further details on the component and test methods are provided in Reference [2].

The initial analysis of the test data consisted of calculating the Weibull distributions for each component configuration [3]. When the Weibull distribution was calculated for the previously mentioned BGA56 configuration, the results looked somewhat strange, as shown in *Figure 1*. When cumulative distribution data appear to 'bounce' above and below the best-fit line, as in the figure, it is often the case that the data actually include values from different population characteristics.

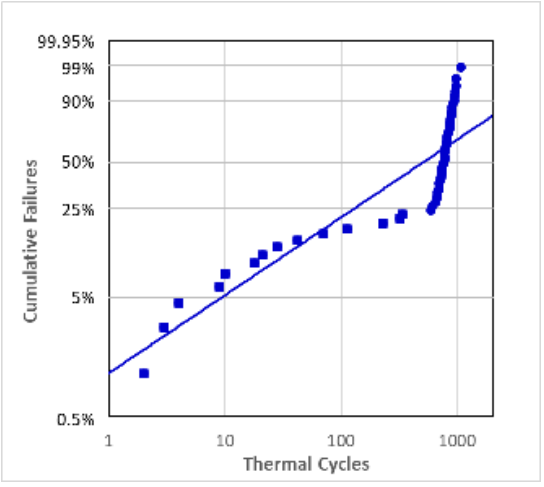

Figure 1 - Cumulative failures of BGA56 components; symbols show measured data, line shows the best fit Weibull distribution

[1] Daisy chain components are custom test devices in which the solder joints are electrically connected together in series, i.e. 'daisy chained', so that if any solder joint fails and creates an electrical open, the failure can be detected.

Table 1 shows the measured failure data for the BGA56 components, grouped by the reference designator, while *Figure 2* shows the same plot as the previous figure, but with the data for the different reference designators indicated with different symbols.

BOARD #	CYCLES TO FAILURE			
	U1	U11	U15	U24
1	10	867	807	859
2	42	651	902	671
3	338	733	612	948
4	18	829	906	850
5	3	886	591	856
6	21	814	759	793
7	112	657	773	692
8	322	730	746	699
9	724	776	771	945
10	4	673	804	692
11	228	754	817	970
12	28	813	773	896
13	71	966	716	1071
14	9	885	774	720
15	2	964	865	837

Table 1 - Measured failure data

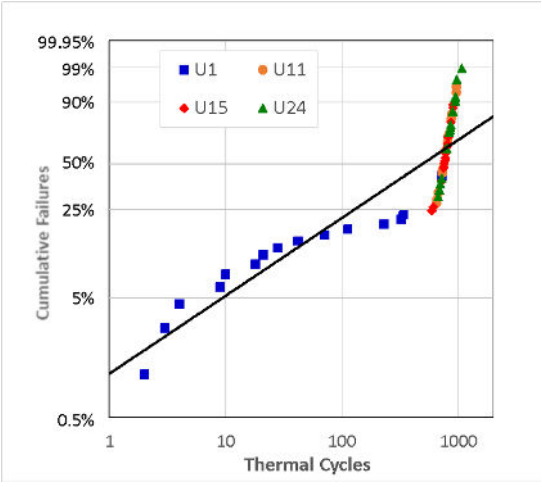

Figure 2 - Cumulative failures of BGA56 data plotted for different component reference designators

Simple observation of either the raw or the plotted data should be sufficient to make one suspect that the reliability of the U1 components was substantially different from the others. For quantifiable indications of whether there are differences between U1 and the other components, we could plot individual sets of data for each reference designator, as shown in *Figure 3*.

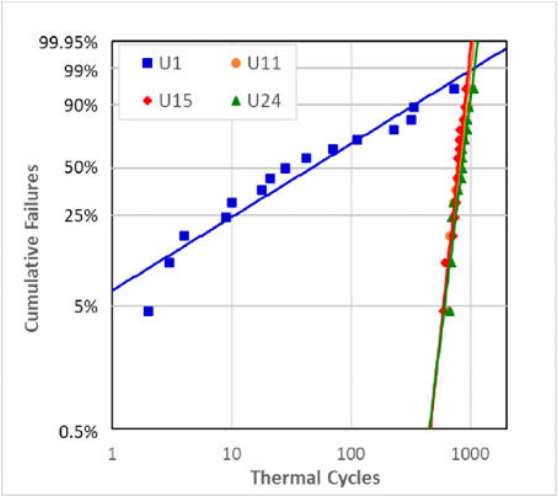

Figure 3 - Cumulative failure distributions for BGA56 components, segregated by different component reference designators

In addition, since all the components in consideration failed by the end of testing, we can assume that they followed a roughly normal distribution and compare the means using a t-test [4]. Results of using a t-test to determine the probability that two populations have the same means are summarized in *Table 2*. Combinations with values less than 5% would typically be considered a statistically significant indication that the populations are different. As shown in this table results from U1 appear to be significantly different from the other components, but there is no statistically significant difference between any of the other combinations; for example, the t-test between U11 and U24 produced a value larger than 5% (of 42.1%).

	U1	U11	U15
U24	0.0%	42.1%	14.0%
U15	0.0%	47.2%	
U11	0.0%		

Table 2 - Results of t-tests that compare data sets in Table 1

	β (value & range)		Θ (value & range)	
ALL	0.66	0.52 – 0.79	859	34 – 1.11e5
U1	0.60	0.54 - 0.66	85	40 - 214
U11	8.71	7.9 - 9.52	844	269 - 3357
U15	9.26	8.34 - 10.2	816	245 - 3540
U24	7.82	6.89 - 8.75	888	211 - 5519

Table 3 - Regression analysis coefficients for 80% confidence level

Alternatively, or if all of the components had not failed by the end of testing, we could compare the coefficients for the Weibull distributions of the different populations. Since the coefficients (β and θ, which as a reminder, are similar to the standard deviation

and mean of a normal distribution) are calculated using linear regression, we can determine the uncertainty of the values for a given confidence level [5]. The results of this analysis are shown in *Table 3*; the 'range' values indicate the values in which one is 80% confident that the values of β and θ are within. This table shows substantial differences in the calculated coefficients and their ranges for the selected confidence level.

Dedicated readers of this column are invited to review references [3-5] and duplicate the results shown in *Table 2* and *Table 3*.

After it was recognized that there was such a significant difference in the results for the U1 components than the others, efforts were made to determine the source of the difference. Inspections of micrographic cross-sections of failed parts revealed that U1 components consistently had a single solder joint with insufficient solder. Eventually, it was determined that an error had been made in the design of the solder stencil used to apply solder to the test board prior to part placement and solder reflow. This led to no solder paste being applied to the solder pad, which produced a solder joint that was doomed to fail far earlier than it should have. This was an example in which the statistical analysis revealed a problem with the testing approach. Fortunately, because of the nature of thermal cycling to evaluate solder joint reliability, there were ample opportunities to assess the components after the fact and identify the root cause. In other types of testing, it may be difficult to determine a true root cause if the nature of the test does not leave as many 'bread crumbs' to determine what happened. That may lead to the need to repeat a test.

Sometimes we don't have an entire set of data that is questionable, but just one odd result. Can we just throw out the data we don't like? Well, we probably shouldn't…. But if data are drawn from a population that truly is a normal distribution, it is certainly possible to occasionally have a measurement that is 4 or 5 (or more) standard deviations from the mean. These types of outliers may be real – but they may not provide a good indication of the true population, particularly if we have only a few measurements. Chauvenet's Criterion can be used to assess whether a single data point is an outlier and provides a formal method that can justify eliminating a data point that seems to be an outlier [5]. The Chauvenet test statistic, τ, is defined in *equation 1*:

$$\tau = |x-\mu|/\sigma \quad (1)$$

where x is the suspicious value, μ and σ are, respectively, the mean and standard deviation of the population. The value of τ depends on the number of measurements made in the population, as shown in *Table 4*. The test statics in the table can be calculated with Excel using the function "abs(norm.s.inv(1/(4*n)))".

To use the Chauvenet Criterion to assess an outlier data point, calculate the mean and standard deviation of the full data set (including any suspected outliers) and then calculate the value of τ as shown in *equation 1*. If that value is larger than the test statistic shown in *Table 4* for the population size, that outlier data point can be removed so that the average and standard deviations can be determined without it.

n	τ
3	1.383
4	1.534
5	1.645
6	1.732
7	1.803
8	1.863
9	1.915
10	1.960

Table 4 - Chauvenet test statistics

For example, I recently tested thermoelectric cooler (TEC) devices to measure their performance characteristics. This was done with an existing thermal test stand that required that two TECs be tested and averaging the performance of both. As part of this testing, I conducted repeated tests of the same TECs to better understand the measurement variability. The same pair of TECs was tested six times and the average Q_{max} value, which is the maximum heat that can be input to the TEC while maintaining zero temperature difference on the two sides.

The six measured values for Q_{max} are shown in the $x_{original}$ column of *Table 5*, with average and standard deviation values of 4.833 and 0.290. The normalized deviation is calculated by finding the absolute value of the difference between a value and the mean and then normalizing it by the standard deviation. The measurement of 4.33W has a deviation of 1.91, which is larger than the value of τ for n = 6 of 1.732, as shown in *Table 4*. Therefore, we can use the Chauvenet criterion to eliminate that one data point and assume our data set is that shown in the $X_{updated}$ column.

	$x_{original}$	$(x-\mu)/\sigma$	$x_{updated}$
measured values for Q_{max} (W)	5.13	0.85	5.13
	4.95	0.23	4.95
	4.83	0.18	4.83
	4.33	1.91	
	4.99	0.37	4.99
	5.07	0.64	5.07
mean, μ	4.883		4.994
st dev, σ	0.290		0.115

Table 5 - TEC Measurements and Data Analysis

Figure 4 plots the data and shows the impact of applying the Chauvenet Criterion. Eliminating the single outlier actually did

not change the average value much (increasing it by 2.3%). The main impact of applying the Chauvenet Criterion was on the standard deviation, which is reduced by more than 60%.

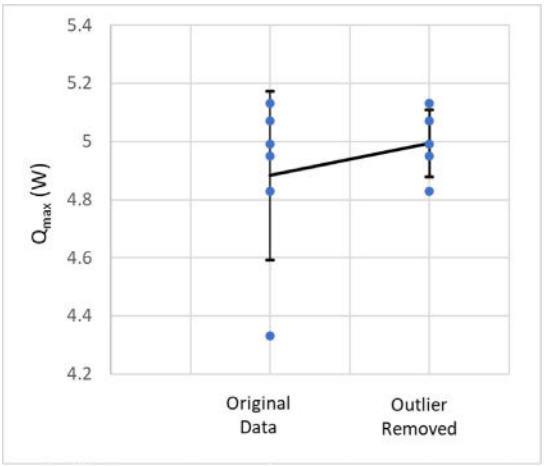

Figure 4 - TEC data before and after removing one data point using Chauvenet's Criterion. Error bars indicate one standard deviation.

Summary

Statistical analysis is not simply a process of plugging data into a set of equations and reporting the results. It is important that the analyst pays attention to the data to try to detect values that could be problematic and lead to incorrect conclusions. In some cases, a statistical analysis can detect results that do not accurately characterize the true population and help to guide the researchers to review their test approach to identify an experimental error. In other cases, testing may not have left any 'breadcrumbs' that can be used to find direct evidence of why a data point is an outlier. As a general rule, data should not be simply discarded because it is inconvenient, but methods such as Chauvenet's Criterion do at least provide a formal method that can help to justify removing a measurement that excessively increases the measured variance.

References

[1] Dave Hillman, et al. "The last will and testament of the BGA void", Journal of Surface Mount Technology, July-Sept 2012, Vol. 25, Is. 3, pp. 29 – 41
[2] Ross Wilcoxon, "Statistics Corner: Weibull Distribution", Electronics Cooling Magazine, Jan. 2023.
[3] Ross Wilcoxon, "Statistics Corner: Comparing Populations", Electronics Cooling Magazine, Sept. 2023.
[4] Ross Wilcoxon, "Statistics Corner: Regression Analysis", Electronics Cooling Magazine, Mar. 2022.
[5] J.P. Holman, "Experimental Methods for Engineers, 6th edition", McGraw-Hill, 1994, pp. 73-75

Index of ADVERTISERS

Electronics Cooling

t: 484.688.0300
e: info@electronics-cooling.com
w: www.electronics-cooling.com
page: 25

LECTRIX

t: 484.688-0300
e: info@lectrixgroup.com
w: www.lectrixgroup.com
page: 31

Leader Tech Inc.

t: 866.832.4364
e: sales@leadertechinc.com
w: www.leadertechinc.com
page: 2

SIEMENS Digital Industries Software

t: 800.592.2210
e: www.plm.automation.siemens.com/global/en/contact-us.html
w: www.plm.automation.siemens.com/global/en/
page: 5

SEMI-THERM

t: 408.840.2354
w: www.semi-therm.org
page: 8


Break the same old pattern.
Problem First. Product Last.
Content | Data | Marketing Technology
LECTRIX®
Digital Marketing for the B2B Electronics Industry
1.484.688.0300 | info@lectrixgroup.com
www.lectrixgroup.com